Talanta 228 (2021) 122230

Contents lists available at ScienceDirect

Talanta

journal homepage: www.elsevier.com/locate/talanta

Enhanced electrochemiluminescence cytosensing based on abundant oxygen vacancies contained 2D nanosheets emitter coupled with DNA device cycle-amplification

Huan Gao [a], Junfang Zhang [a], Xuan Wei [a], Qinshu Zhu [a,**], Tianxiang Wei [a,b,*]

[a] Jiangsu Collaborative Innovation Center of Biomedical Functional Materials and Jiangsu Key Laboratory of Biofunctional Materials, School of Chemistry and Materials Science, Nanjing Normal University, Nanjing, 210023, People's Republic of China
[b] School of Environment, Nanjing Normal University, Nanjing, 210023, People's Republic of China

ARTICLE INFO

Keywords:
Electrochemiluminescence
Oxygen vacancies
2D nanosheets emitter
Signal amplification
Cytosensing

ABSTRACT

Developing efficient and sensitive cytosensing method has great significance for the detection of low abundant circulating tumor cells (CTCs). Electrochemiluminescence (ECL) biosensor, as an attractive analytical tool, has shown a great potential in sensitive cell counting. Its detection efficiency is strongly dependent on the electrochemiluminescent materials, whose property is related to its morphology and surface vacancies. Herein, the ultrathin Lu_2O_3–S nanosheets contain abundant oxygen vacancies were newly synthesized. Its special two-dimensional (2D) structure morphology and surface vacancy endowed it intensified and stable ECL emission. The possible mechanism was deduced from experiments and discussed. Then, through integrating with a DNA device cycle-amplification system plus signal conversion pretreatment, we constructed a crossed enhanced ECL cytosensing platform. In this system, the target cells were transformed into programmable sequences, which could be next coupled with DNA device cycle-amplification on the modified electrode surface. Using Ag_2S quantum dots as the energy acceptor toward Lu_2O_3–S donor, and CCRF-CEM cells (CEM) as the model CTCs, an enhanced ECL cytosensing platform was proposed, displaying good analytical performance for acute lymphoblastic leukemia cancer cell detection. The ECL signal responded proportionately on the CEM cells concentration in a wide range of 5×10 to 1×10^6 cells/mL, and a low detection limit of 10 cells/mL was obtained. This work provided an alternative way to design high-performance ECL luminophores, and also would be an effective solution for CTCs counting.

1. Introduction

Cancer is a malignant disease with high fatality rate. The detection of cancer biomarker is of great significance for achieving precise medicine and reducing mortality [1,2]. Circulating tumor cells (CTCs) as one of important cancer markers, whose expression level is closely related to tumor stage diagnosis and therapy [3–6]. While, the number of CTCs is extremely rare in the peripheral blood of patients, which is a great challenge for sensitive analysis and specific diagnosis [7]. Hence, the development of sensitive cytosensing method of CTCs is essential towards timely diagnosis and treatment of cancer patients. Compared with the other reported efficient methods for CTCs counting, like photoluminescence (PL) [8], electrochemical impedance spectroscopy (EIS) [9], and linear sweep voltammetry [10], electrochemiluminescence (ECL) assay exhibits remarkable characteristics including high sensitivity, low cost and low background noise [11].

For the construction of ECL cytosensing platform, developing highly efficient and robust emitters plays a key role in the improvement of ECL analytical performance. Studies have shown that the ECL emission is manifested as direct annihilation of the electrogenerated radical-ion (anion and cation) [12]. For the mostly used ECL emitters-semiconducting materials, the annihilation process is closely related to electron-hole recombination and high-energy electron transfer reaction of the surface states. Therefore, the ECL properties can be modulated by tuning the recombination dynamics of excited charge carriers like morphology and surface vacancies [13–15].

* Corresponding author. Jiangsu Collaborative Innovation Center of Biomedical Functional Materials and Jiangsu Key Laboratory of Biofunctional Materials, School of Chemistry and Materials Science, Nanjing Normal University, Nanjing, 210023, People's Republic of China.
** Corresponding author.
E-mail addresses: zhuqinshu@njnu.edu.cn (Q. Zhu), weitian_xiang@126.com (T. Wei).

https://doi.org/10.1016/j.talanta.2021.122230
Received 7 December 2020; Received in revised form 6 February 2021; Accepted 13 February 2021
Available online 19 February 2021

Over the past few decades, various morphologies of advanced electrochemiluminophores with efficient ECL property applied in biosensing have been subjected to extensive studies, including nanotubes [16], nanoclusters [17], core@shell nanoparticles (NPs) [18], etc. Among all these choices, two-dimensional (2D) nanomaterials have been considered as some of the most attractive candidates due to their unique physicochemical properties that emerge upon low dimensionalities, which possess the characteristic of high carrier mobility and large-area uniformity [19]. And the ultrathin planar structure of nanosheets provides abundant responsive points for the immobilization of active molecules [20]. The intensive efforts for graphene-like layered materials have been contributed, like transition-metal materials [21,22], which exhibit good performance in ECL biosensing detection. Lately, rare earth nanomaterials have drawn our attention due to their intrinsic luminescence properties and super biological compatibility [23]. Some attempts have been tried to develop diverse morphologies with rare earth elements composition. For example, Shi's group harnessed upconversion nanoparticles@g−C_3N_4 to accomplish multifunctional luminescent materials [24]. Chen's group aimed at the issue of designing novel ECL emitter one dimensional europium hydroxide nanorods and proposed a bioanalysis for detection of thrombin [25]. Also, we have previously studied the effect of different morphologies of S-doped Y_2O_3 on ECL properties [26]. It was found that the structure of nanosheet exhibited better ECL performance and stability than nanowires. All the mentioned above inspired us that 2D rare earth nanomaterial might serve as a good ECL luminophore candidate.

Apart from the tailoring of morphology, the surface vacancy is also a key point to intensify the performance of ECL luminophores. Some considerable synthesized approaches have been studied, including doping [27], hybridization [28], and encapsulation [29], which have shown great potential for modulating defects and exhibited the improvement in device fabrication, photocatalysis and biological applications. Among them, heteroatom doping is widely used because it can effectively tune the charge distribution, create more surface vacancies and increase carrier mobility [30]. However, the correlational research in ECL field is just getting started [31–33].

Accordingly, we expect to prepare a novel rare earth 2D structure emitter through adopting the method of heteroatom doping to modulate its surface defects for obtaining enhanced ECL performance and better cytosesing system. In this work, ultrathin Lu_2O_3–S nanosheets with abundant oxygen vacancies and strictly defined 2D confinement were newly synthesized and adopted as the desired electrochemiluminophores. On this basis, a sensitive ECL cytosensing was established. CCRF-CEM (CEM) cells as one kind of CTCs were chosen as model analyte in the following research, which also is an essential biomarker of life-threatening acute lymphoblastic leukemia (ALL) [34,35]. For achieving higher sensitivity towards the low abundance CEM cells, we designed a cross-platform sensing system, which integrated DNA device cycle-amplification technology to convert few CEM cells into plenty of copyDNAs.

Based on a Lu_2O_3–S/Ag_2S ECL resonance energy transfer (ECL-RET) pair and signal conversion pretreatment of CEM cells, an enhanced ECL cytosensing was developed (Scheme 1). Firstly, through DNA hybridization-competition strategy, aptamers (sgc8c) modified Au NPs were attached to the surface of CEM cells where the membrane protein tyrosine kinase-7 (PTK7) specifically bound to sgc8 aptamers is overexpressing [36]. Meanwhile, most complementary sequences (intermediate DNA) were released, CEM cells were converted to intermediate DNAs (Scheme 1A). Compared with target cells, the alternative DNA sequences can retain bioactivity for a longer time. Besides, they are more stable and maneuverable for signal amplification and can serve as a new targeting element in the following ECL detection system. Then, as shown in Scheme 1B, ultrathin Lu_2O_3–S nanosheets modified electrode exhibited a very strong ECL signal. $S(sequence)_{12}$ and S_{34}–Ag_2S were attached to the electrode surface, which were consist of S1 and S2, S3–Ag_2S and S4 by normal complementary base pairing, respectively. S2 was used to restrict the hybridization between S1 and S_{34}–Ag_2S. When Ag_2S quantum dots (QDs) located in the vicinity of the electrode surface, a decreased ECL response was caused due to the ECL-RET effect [37,38]. Then the intermediate DNA and T7 exonuclease (T7 exo) were incubated in the reaction solution. The former hybridized with S2 and released S1. The latter digested the blunt of hybrids and sheared S3–Ag_2S into pieces. Concurrently, S1 was released and recycled. The ECL signal would recover and the quantitative detection of CEM cell was achieved. As a result, based on ultrathin Lu_2O_3–S nanosheets with abundant oxygen vacancies, an enhanced ECL cytosensing platform was constructed and exhibited a good analysis performance. The ECL property is influenced by the rate of electron-hole recombination and high-energy electron transfer of the surface states, which can be modulated by morphology and surface vacancies. We expected that synergistically tailoring of morphology and surface vacancies of emitter would lead to an enhancement of ECL property. A proof-of-concept was conducted by successfully synthesize 2D Lu_2O_3–S ultrathin nanosheets with abundant oxygen vacancies, which showed an intense and stable ECL intensity, making it a good ECL emitter. Then, combined with DNA device cycle-amplification, a sensitive and specific CTCs counting method was proposed. Compared with other functional based optical materials-dependent sensor, for example, the ligand based innovative

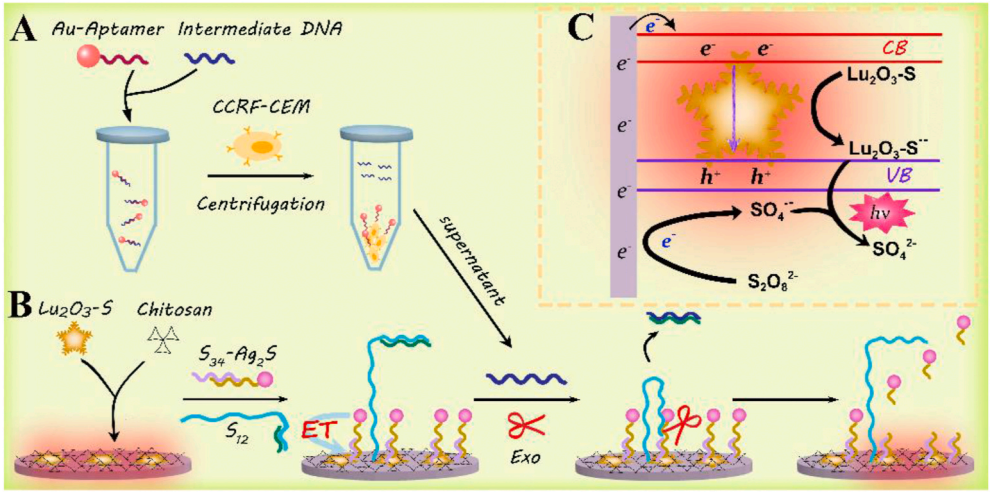

Scheme 1. Illustration of (A) the signal conversion pretreatment process, (B) the ECL cytosensing based on abundant oxygen vacancies contained ultrathin Lu_2O_3–S nanosheets coupled with DNA device cycle-amplification for the detection of CEM cell, and (C) the ECL emission mechanism of the ultrathin Lu_2O_3–S nanosheets.

composite material-dependent sensors, which attracted our attention for their functionality [39,40], high surface area [41,42], mechanical stability [43,44], the proposed sensor has a higher sensitivity. While, the reversibility and reusability of materials need to be improved [45,46]. Besides, this work may provide a new thought in the design of ECL luminophores and the detection of clinical tumor cells.

2. Experimental section

2.1. Materials and chemicals

Lutetium chloride hexahydrate ($LuCl_3{\cdot}6H_2O$, ≥99.9%), oleic acid (OA) and dodecylamine (DDA, 98%) were purchased from Aladdin (Shanghai, China). $AgNO_3$, thiourea (H_2NCSNH_2, >99%), KH_2PO_4, Na_2HPO_4, KCl, NaCl, $K_2S_2O_8$, $K_4Fe(CN)_6$, $K_3Fe(CN)_6$, acetic acid, ethanol, n-heptane were gained from Sinopharm Chemical Reagent Co., Ltd. (China). Chitosan, ethylene glycol, N-(3-dimethylaminopropyl)-N′-ethylcarbodiimide (EDC), N-hydroxysuccinimide (NHS, 98%), monoethanolamine (MEA) and 1-octadecene (ODE, 90%) were purchased from Sigma-Aldrich Inc. (USA). Tris(hydroxymethyl)aminomethane (Tris), 3-mercaptopropionic acid (MPA) and glutaraldehyde (GA, 25%, v/v) were supplied by Alfa Aesar Ltd. (China). Phosphate buffer saline (PBS, 10 mM, pH = 7.4) was used to resuspend cells. Tris-HCl buffer (10 mM, pH = 7.4) was employed as washing solution and dissolving S1 and S2. PBS buffer (0.1 M, pH = 7.4) containing 50 mM $K_2S_2O_8$ was used as testing electrolyte solution. All high-performance liquid chromatography (HPLC)-purified sequences (Table S1) in our experiments were synthesized and purchased from Sangon Biotech Co., Ltd. (Shanghai, China). CEM cells (T cell line, human ALL) and Ramos cells (B cell line, human Burkitt's lymphoma) were obtained from Keygen Biotech Co., Ltd. (JiangSu, China). T7 exo and NE Buffer 4 were provided by New England BioLabs Ltd. (Beijing, China).

2.2. Apparatus

The ECL tests and cyclic voltammetry (CV) responses were performed and obtained synchronously by a classical three electrodes system with MPI-A system (Remex Analytical Instrument Co., Ltd., Xi'an, China) at room temperature. The three electrodes system containing a modified glassy carbon electrode (GCE, 4 mm diameters) as working electrode, a Ag/AgCl electrode (3 M KCl) as reference electrode and a Pt-rod as counter electrode. EIS spectra were acquired on Autolab potentiostat/galvanostat PGSTAT302 N (Metrohm, Netherlands) with 10 mV signal amplitude and frequency scan range from 0.1 Hz to 100 KHz. The electrolyte solution was 100 mM KCl containing $K_3Fe(CN)_6$:$K_4Fe(CN)_6$ (1:1, 5 mM) mixture. The Powder X-ray diffraction (PXRD) pattern was performed by means of a D/max 2500VL/PC diffractometer (Japan) with graphite monochromatized Cu Kα radiation (2θ, from 20 to 90°). The high-resolution transmission electron microscope (HRTEM, JEOL-2100F, Japan) was taken to characterize morphology and elemental mapping with an accelerating voltage of 200 kV. The PL spectrum was acquired on Fluoromax-4 spectrofluorometer (Horiba, USA). The UV–vis absorption spectra were carried out with Cary 60 spectrophotometer (Agilent, USA). The X-ray photoelectron spectroscopy (XPS) data were recorded on a scanning X-ray microprobe (PHI 5000 Verasa, ULACPHI, Inc.) with Al Kα radiation. Inductively coupled plasma (ICP) data were acquired on an Inductively Coupled Plasma Atomic Emission Spectrometer (Jarrell-Ash 1100 + 2000). Atomic force microscopy (AFM) image was obtained on a Bruker Dimension Icon instrument.

2.3. Synthesis of ultrathin Lu_2O_3–S nanosheets

The Lu_2O_3–S nanosheets were synthesized via the one-pot-method. Specifically, 1 mmol of $LuCl_3{\cdot}6H_2O$ (0.3894 g) and 4 mmol of H_2NCSNH_2 (0.3045 g) were mixed with OA (4 mL), OLA (5 mL) and ODE (5 mL) in a 250 mL three-necked flask. The reaction system was heated to 280 °C at 7 °C·min^{-1} and maintained at this temperature for 1 h. After the reactor cooling down to room temperature, the product was washed four times using n-heptane and ethanol (1:1, v/v), and dried at 40 °C for 6 h.

2.4. Synthesis of Ag_2S QDs

Ag_2S–COOH QDs were synthesized based on previous reports [47]. The as-obtained Ag_2S QDs were dispersed in water and stored at 4 °C.

2.5. Synthesis of water-soluble Au NPs

Au NPs were synthesized based on previous report [48]. The prepared Au NPs solution was stored at 4 °C for further use.

2.6. Signal conversion pretreatment

This strategy can realize the signal conversion from target cells to copyDNAs. 4 μM of aptamer (100 μL) and Au NPs (50 μL) were mixed evenly in eppendorf tube and kept at 4 °C overnight. Then the suspension was discarded by centrifuged at 10,000 rpm for 4 min. Followed by adding 4 μM of intermediate DNA (200 μL) into the mixture and maintained at 37 °C for 1 h. The unbonded sequences were removed at 10,000 rpm for 4 min. Subsequently, 150 μL of PBS containing different concentrations of cells was added and incubated at 37 °C for 1 h. After the above process, the mixture was centrifuged at 2000 rpm for 3 min to separate CEM cells and obtained the intermediate DNA. Before being added into the ECL detection system, the supernatant needed to be centrifugated again for separating the unconnected Au NPs.

2.7. Preparation of S3–Ag_2S

Under the activation of EDC and NHS, S3 was immobilized onto the surface of Ag_2S QDs via classical coupling reaction between amino groups of S3 and carbonyl groups of Ag_2S QDs at 37 °C for 1 h (the concentration of S3 is 10 μM in final volume).

2.8. Preparation of S_{12} and S_{34}

1 μM of S1 and 2.5 μM of S2 were mixed (1:1, v/v) and heated at 95 °C for 5 min, then the mixture was naturally cooled down to room temperature for obtaining S_{12}. Following the same steps, 10 μM of S3–Ag_2S and 20 μM of S4 were mixed (1:1, v/v) and reacted to get S_{34}.

2.9. Fabrication of the ECL cytosensing

The GCE was polished by 0.05 μm alumina powders and washed four times with ethanol and water. Then dried by N_2 before 1 mg mL^{-1} Lu_2O_3–S nanosheets (15 μL) were spread onto the surface. After being dried under room temperature, 0.1 wt % chitosan-acetic acid solution (5 μL) was affixed to the electrode surface and dried overnight. Therewith the electrode was immersed into GA solution (600 μL, 2.5%, v/v) at 25 °C for 1 h and rinsed with washing solution. Subsequently, the mixture of S_{12} and S_{34}–Ag_2S (15 μL, 1:1, v/v) was incubated and immobilized on the electrode surface at 37 °C for 1 h. The modified electrode was washed to remove the unbound sequences. The nonspecific adsorption sites of the electrode surface were blocked by MEA solution (15 μL, 500 μM) at 25 °C for 1 h. After that, the electrode was further incubated with T7 exo, (100 U/mL), NE Buffer 4 (1 ×) and the supernatant (10 μL) from signal conversion pretreatment containing the intermediate DNA at 25 °C for 2 h. Finally, the electrode was rinsed with NE Buffer 4 (1 ×) and carried out the ECL measurement at the voltage of the photomultiplier tube of 800 V (potential range: −2.0 - 0 V, scan rate: 100 mV s^{-1}).

2.10. Cell culture and treatment

CEM cells and Ramos cells were cultured in cell culture flask and placed in a humidified incubator (5% CO_2, 37 °C). The culture medium is RPMI 1640 containing penicillin (80 U mL^{-1}) and streptomycin (0.08 mg mL^{-1}) supplemented with 10% fetal bovine serum. When cells grew to the logarithmic growth phase, they were separated from the culture medium by centrifugation at 1000 rpm for 5 min. Then the cell sediment was resuspended gently in the sterile PBS buffer (10 mM) to obtain a homogeneous suspension. The number of cells in suspension was counted with a hemocytometer.

3. Results and discussion

3.1. Characterization of materials

TEM is an analytical technique that directly visualize the morphology of materials [49,50]. The 2D structure and nearly transparent image of Lu_2O_3–S nanosheets were characterized by TEM and AFM (Fig. 1A and B), which clearly showed the planar morphology and ultrathin thickness of Lu_2O_3–S nanosheets. The thickness diagram of the Lu_2O_3–S nanosheets is approximately 5.02 nm (Fig. 1C). The diffraction peaks in XRD pattern of Lu_2O_3–S nanosheets corresponding to Lu_2O_3 (JCPDS 43–1021) (Figure S1), which confirmed the crystalline phase of this material. As shown in Fig. 1D, three elements of Lu, S and O in elemental mapping were expressed by three different colors, which illustrated that each component was distributed uniformly. Besides, the newly prepared Lu_2O_3–S nanosheets showed a greatly enhanced ECL intensity in Fig. 2A, and the initial potential is −1.5 V. Also, it presented the relatively stable ECL signal over eleven cycles (Fig. 2B), and the relative standard deviation (RSD) was 1.5%, demonstrating that it has persistent emission. The excellent ECL performance may be attributed to chemical doping, which can effectively modulate surface state and create more oxygen vacancies [51]. To verify this hypothesis, XPS and ICP were employed to determine the surface electronic structures and components of elements. Fig. 2C revealed O 1s XPS spectra of Lu_2O_3–S nanosheets. The three deconvoluted peaks of O 1s each represented different oxygen states: surface oxygen vacancies (c, 531.6 eV), surface absorbed oxygen (b, 530.7 eV), and lattice oxygen (a, 529.0 eV) [52–54]. The obtained surface oxygen vacancies ratio of Lu_2O_3–S nanosheets is calculated to be 40.31%, this data confirmed our inference that more oxygen vacancies may result in good ECL performance. Then, the molar ratio obtained from ICP tests were shown in Table S2. The molar ratio of sulfur from Lu_2O_3–S nanosheets is approximately 12.36%. As the higher ratio content of heteroatom in materials surface may introduce more surface oxygen vacancies [55,56], higher heteroatom doping in our Lu_2O_3–S nanosheets introduced more surface oxygen vacancies, which led to the enhanced ECL performance. Besides, the morphologies of hydrophilic Ag_2S QDs and Au NPs were characterized using TEM, approximately 6 nm and 13 nm in width, respectively (Figure S2).

3.2. The possible ECL emission mechanism of Lu_2O_3–S nanosheets

To investigate the possible ECL mechanism of Lu_2O_3–S nanosheets, ECL and CV characteristics of GCE and Lu_2O_3–S nanosheets modified GCE were carried out. The cyclic potential scanning is conducted from −2.0 to 0.0 V. The CV curve in Fig. 3A represents redox response of bare GCE in PBS buffer (0.1 M, pH = 7.4) containing 50 mM $K_2S_2O_8$. An obvious cathode peak at −1.25 V indicated the production and radiative deactivation of co-reactant. The corresponding ECL curve below shows a peak at 2.0 V with the ECL intensity about 1800 au. Fig. 3B and C shows CV and ECL curves of Lu_2O_3–S nanosheets modified GCE in PBS buffer without or with the addition of $K_2S_2O_8$. The CV profile of the former displays a reduction peak at about −0.5 V and −1.7 V, in which shows little or no ECL signal. Compared with bare GCE, the reduction peak of CV curve of Lu_2O_3–S nanosheets modified GCE is clearly negative shift (−1.67 V), indicating that Lu_2O_3–S nanosheets also participated in redox reaction [57,58]. Furthermore, a strong ECL signal was observed in Fig. 3C, which might come from the following redox co-reactant pathway (Scheme 1C): during cathodic potential scan, the working electrode provided electrons for activating Lu_2O_3–S nanosheets. Then, the electrons were injected into the conduction band (CB) of Lu_2O_3–S nanosheets and produced Lu_2O_3–S^- (Eq. (1)). Simultaneously, lots of $S_2O_8^{2-}$ were electro-reduced into $SO_4^{\cdot-}$ (Eq. (2)). These two radicals, Lu_2O_3–S^- and $SO_4^{\cdot-}$, reacted with each other and generated the excited state Lu_2O_3–S* (Eq. (3)), which decayed back to the ground state with the ECL emission (Eq. (4)). The equations of ECL emission mechanism

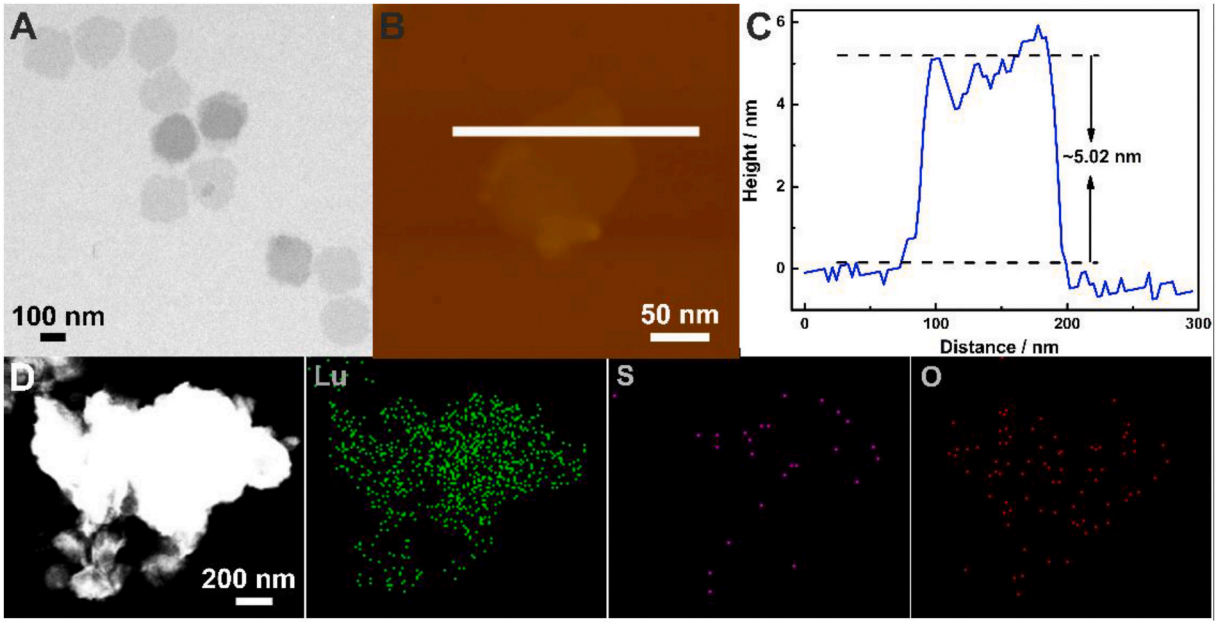

Fig. 1. (A) TEM image, (B) AFM image of Lu_2O_3–S nanosheets and (C) the corresponding diameter and thickness diagram; (D) Elemental mapping of Lu_2O_3–S nanosheets.

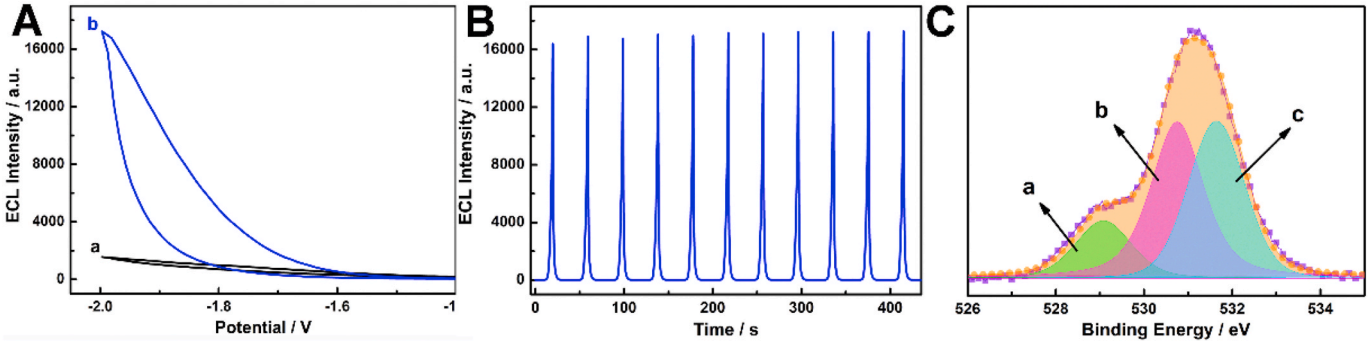

Fig. 2. (A) ECL potential curves of GCE (a) and Lu_2O_3–S nanosheets modified GCE (b) in PBS buffer (0.1 M, pH = 7.4) containing 50 mM $K_2S_2O_8$; (B) ECL stability test of Lu_2O_3–S nanosheets modified GCE under eleven cyclic potential scans; (C) The XPS spectra of Lu_2O_3–S nanosheets for O 1s (a, b and c represent lattice oxygen, surface absorbed oxygen and surface oxygen vacancies, respectively).

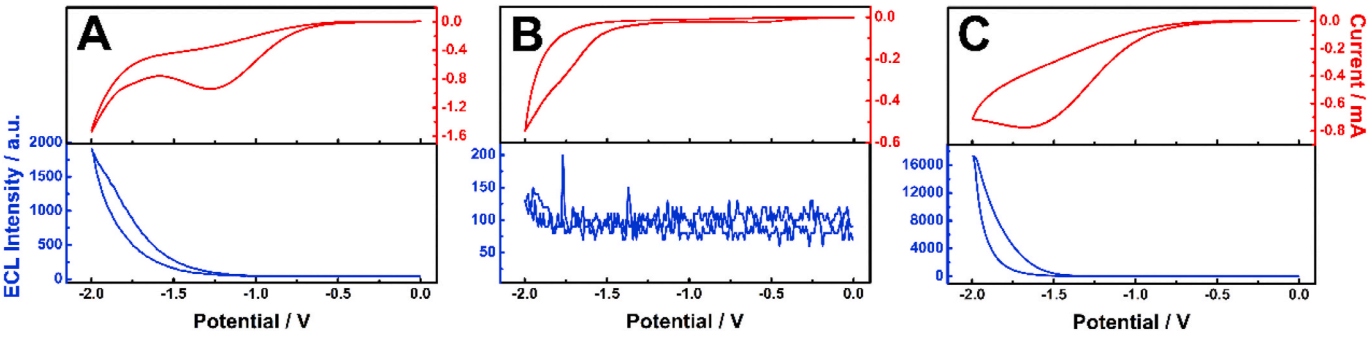

Fig. 3. ECL intensity-potential plots and the corresponding CV profiles of (A) bare GCE in PBS buffer (0.1 M, pH = 7.4) containing 50 mM $K_2S_2O_8$, (B) Lu_2O_3–S nanosheets modified GCE in PBS buffer, and (C) Lu_2O_3–S nanosheets modified GCE in PBS containing 50 mM $K_2S_2O_8$.

are proposed as follows [59]:

$$Lu_2O_3\text{–}S + e^- \rightarrow Lu_2O_3\text{–}S^- \quad (1)$$

$$S_2O_8^{2-} + e^- \rightarrow SO_4^{2-} + SO_4^- \quad (2)$$

$$Lu_2O_3\text{–}S^- + SO_4^- \rightarrow Lu_2O_3\text{–}S^* + SO_4^{2-} \quad (3)$$

$$Lu_2O_3\text{–}S^* \rightarrow Lu_2O_3\text{–}S + h\nu \quad (4)$$

3.3. Characterization of the ECL cytosensing

In addition to the efficiency of electrochemiluminophores, the analysis capability of this cytosensing is also influenced by the feasibility of the ECL-RET effect between Lu_2O_3–S nanosheets and Ag_2S QDs. Apparently, emission spectrum of Lu_2O_3–S nanosheets and absorption spectrum of Ag_2S QDs showed a spectral overlap, suggesting that the ECL-RET effect may be gained successfully (Fig. 4A). Also, to effectively verify that aptamers were successfully connected to the surface of Au NPs, UV–vis absorption spectra were investigated (Fig. 4B). Au NPs and aptamers showed absorption bands at 520 and 260 nm, respectively. After incubation, the absorption spectrum of the mixture (Au NPs and aptamers) exhibited an obvious absorption band of aptamers at 260 nm, indicating the aptamers were attached to Au NPs.

ECL responses of the cytosensing platform stepwise assembly were recorded (Fig. 5A). A small ECL signal was observed from bare GCE (a).

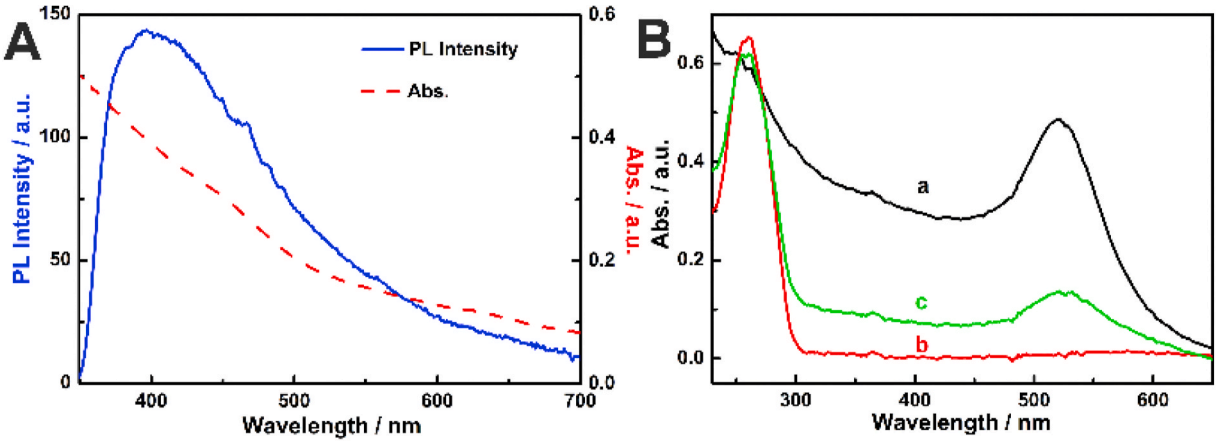

Fig. 4. (A) PL spectrum of Lu_2O_3–S nanosheets (solid line), and UV–vis absorption spectrum of Ag_2S QDs (dotted line); (B) UV–vis absorption spectra of Au NPs (a), aptamers (b), and Au NPs linked with aptamers (c).

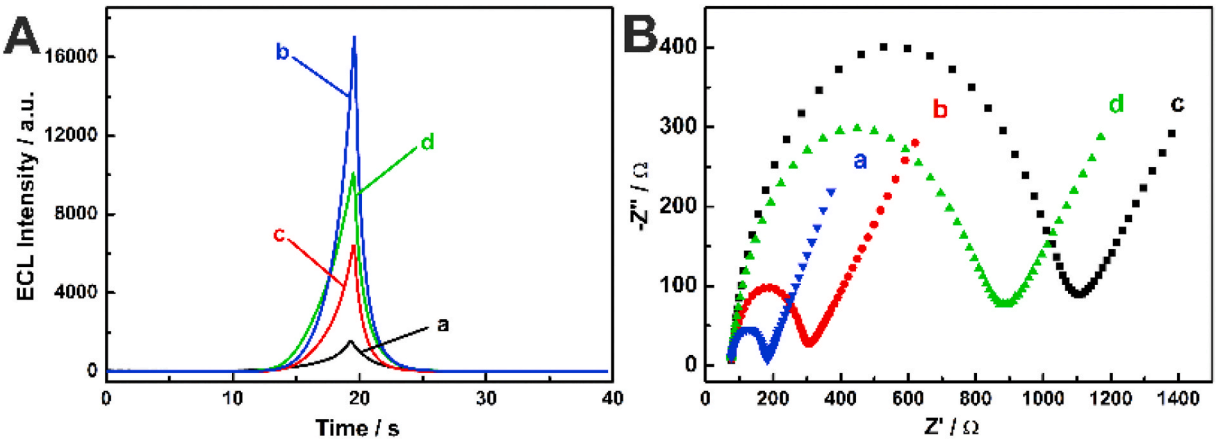

Fig. 5. (A) ECL responses of this cytosensing platform during the layer-by-layer construction process: (a) GCE, (b) Lu_2O_3–S/GCE, (c) S_{12}–S_{34}–Ag_2S/Lu_2O_3–S/GCE, (d) intermediate DNA/S_{12}–S_{34}–Ag_2S/Lu_2O_3–S/GCE (the concentration of CEM cells = 1 × 10^3 cells/mL); (B) Nyquist plots of (a) bare GCE and different modified electrodes: (b) Lu_2O_3–S/GCE, (c) S_{12}–S_{34}–Ag_2S/Lu_2O_3–S/GCE, (d) intermediate DNA/S_{12}–S_{34}–Ag_2S/Lu_2O_3–S/GCE.

After Lu_2O_3–S nanosheets modified on GCE, an enhanced ECL intensity appeared (b), this phenomenon can be attributed to the high efficiency of electrochemiluminophores. When S_{12} and S_{34}–Ag_2S were linked to the electrode surface through amino groups between chitosan and the terminal of double-stranded DNA, the ECL intensity decreased, which was caused by the ECL-RET effect between Lu_2O_3–S nanosheets and Ag_2S QDs (c). The ECL quenching efficiency based on $I_E = 1 - I/I_0$ is calculated to be 62%, which is acceptable. I and I_0 represent the ECL signals of with or without Ag_2S QDs attached to the Lu_2O_3–S modified electrodes, respectively. Then, with the intermediate DNA added into the detection system, the ECL intensity increased (d). The partial recovered ECL signal confirmed the sensitivity and practicability of this cytosensing platform towards CTCs. EIS curves were exhibited in Fig. 5B, which were also utilized to demonstrate the fabrication process of this ECL biosensor. The bare GCE showed a small semicircle due to the slow electron transfer kinetics of redox probe ($Fe(CN)_6^{3-/4-}$), indicating the GCE has small electron transfer resistance (a). When GCE was modified with Lu_2O_3–S nanosheets, an increased semicircle appeared owing to that the materials prevented the way of redox probe access to the electrode surface (b). The electron transfer resistance of the modified electrode was further increased after S_{12} and S_{34}–Ag_2S were decorated on the electrode, which further confirmed that the modification process was successful (c). When the electrode was incubated with the intermediate DNA and T7 exo, S_{34}–Ag_2S was digested by T7 exo and caused a decreased electron transfer resistance (d). The variable EIS plots were consistent with the above ECL tests and verified the construction of the ECL cytosensing.

3.4. Optimal conditions of the ECL cytosensing

During the processes of the biosensing fabrication, many facts may influence the ECL responses. The effects of the concentration of Lu_2O_3–S nanosheets and cleaving time of T7 exo were investigated. Figure S3A showed the varied ECL intensity of GCE modified with different concentrations of Lu_2O_3–S nanosheets. When the concentration of Lu_2O_3–S nanosheets solution increased from 0.1 to 1.0 mg mL^{-1}, the ECL response promoted and reached a maximum at 1.0 mg mL^{-1}, which implied that more electrochemiluminophores could provide more electron-hole pairs and accelerate the ECL process. And when the concentration further increased to 2.0 mg mL^{-1}, the ECL intensity displayed negligible change. Thus, 1.0 mg mL^{-1} was selected as the optimal concentration of Lu_2O_3–S nanosheets. The cleaving time of T7 exo also plays an important role in the detection of CEM cells. The ECL intensity increased with the cleaving time rising from 0.5 to 2 h, and then it slightly decreased at 3 h (Figure S3B). Therefore, 2 h was chosen as the optimal cleaving time for further experiment.

3.5. Analytical performance of the ECL cytosensing

The designed ECL cytosensing was applied to the quantitative determination of CEM cells under the above optimal conditions that the concentration of Lu_2O_3–S nanosheets solution is 1.0 mg mL^{-1} and the optimal cleaving time cleaving time of T7 exo is 2 h. The ECL signals increased with the concentrations of cells suspension varying from 5 × 10 to 1 × 10^6 cells/mL (Fig. 6A b to h). And the corresponding relationship between the ECL response and the concentration of CEM cells was shown in Fig. 6B. The calibration equation was determined as $I = 4584.16 + 1815.16 \lg c$ (c was the concentration of CEM cells, numbers/mL) with a correlation coefficient of 0.9928, the detection limit was calculated at approximately 10 cells/mL with 3σ rule (σ is the standard deviation of the blank after repeated measurements). Compared with other reported assays, the proposed ECL cytosensing platform coupled with DNA device cycle-amplification exhibited better analytical performance based on ultrathin Lu_2O_3–S nanosheets with abundant oxygen vacancies, indicating its good analytical performance (Table S3).

Selectivity, stability and reproducibility are also important parameters to assess the practicality of biological sensors [60,61]. To identify the selectivity of the developed cytosensor, two leukemia cell lines (CEM cells and Ramos cells) were used for the comparison of the ECL signal. Under the same experimental conditions (Fig. 7A), the cytosensing showed little difference in response towards blank and Ramos cells (1 × 10^3 cells/mL). When CEM cells (1 × 10^3 cells/mL) were present, ECL intensity values sharply increased, proving high detection selectivity of this ECL biosensor. This phenomenon can be attributed to the over expression of PTK7 on the surface of CEM cells, which can be specifically recognized by sgc8 aptamers. In view of all above experiments, the proposed ECL cytosensing platform exhibited practical value for target cells detection. And the stability of the ECL cytosensing was examined and presented in Fig. 7B. After consecutive cyclic potential scans for 7 cycles, the ECL intensity of the modified electrode with CEM cells (1 × 10^3 cells/mL) showed a steady trend and the RSD was calculated to be 1.07%. Moreover, the reproducibility of the ECL cytosensing was further estimated by multiple assays. As displayed in Fig. 7C, six modified electrodes with CEM cells (1 × 10^3 cells/mL) were tested and the RSD was calculated to be 2.2%. These experiments testified that the practicality of this cytosensing was acceptable. All obtained data confirmed that our proposed cytosensor showed a good selectivity, long-term stability efficiency and good reproducibility towards CTCs detection. Furthermore, due to the small amounts of reagents used in the experiment, the overall procedure is cost-effective.

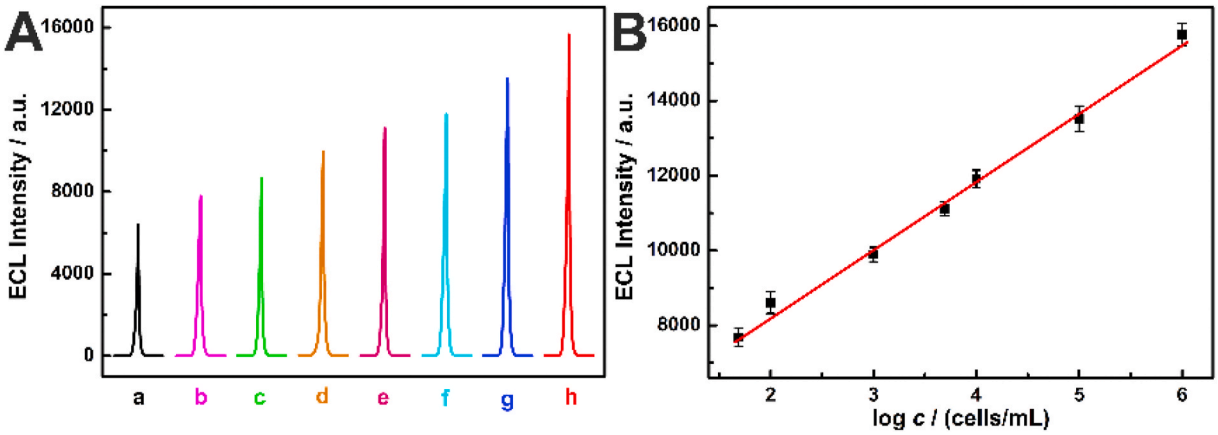

Fig. 6. (A) ECL responses of the cytosensing platform towards CEM cells at different concentrations: (a) 0, (b) 5 × 10, (c) 1 × 10^2, (d) 1 × 10^3, (e) 5 × 10^3, (f) 1 × 10^4, (g) 1 × 10^5 and (h) 1 × 10^6 cells/mL in PBS (0.1 M, pH = 7.4) containing 50 mM $K_2S_2O_8$; (B) The calibration plot about the ECL intensity versus the logarithm value of different concentrations of CEM cells ranging from 5 × 10 to 1 × 10^6 cells/mL.

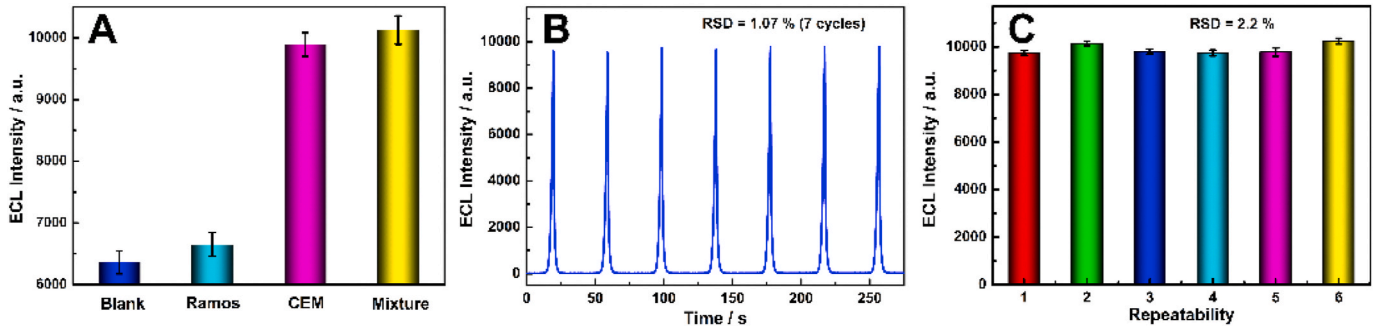

Fig. 7. (A) The selectivity test of the ECL cytosensing platform for the blank, Ramos cells (1 × 10^3 cells/mL), CEM cells (1 × 10^3 cells/mL), and a mixture of CEM cells (1 × 10^3 cells/mL) and Ramos cell (1 × 10^3 cells/mL), (B) The stability of the ECL cytosensing under continuous cyclic potential scans for 10 cycles (1 × 10^3 cells/mL), (C) The reproducibility of the ECL cytosensing (1 × 10^3 cells/mL).

3.6. The application of the ECL cytosensing in real samples

To evaluate the applicability of the ECL cytosensing for real samples, quantitative detection of CEM cells in diluted human serum (Jiangsu Cancer Hospital, China) was carried out. As shown in Tables 1 and 1 × 10^3, 1 × 10^4, and 1 × 10^5 cells/mL of CEM cells were spiked into 100-fold diluted serum samples (by PBS, 10 mM, pH = 7.4) for recovery experiments. The recoveries with different concentrations of CEM cells were measured by the ECL cytosensing. The results within the scope of 98.62%–101.49% with RSD less than 7.89% (n = 3), which is acceptable for the application in real samples.

Table 1
Recovery experiments of CEM cells in 100-fold diluted human serum samples.

Sample number	Added (cells·mL^{-1})	Found (cells·mL^{-1})	Recovery (%)	RSD (%, n = 3)
1	1 × 10^3	1014.90	101.5	7.14
2	1 × 10^4	9989.07	99.89	4.34
3	1 × 10^5	98619.38	98.62	7.89

4. Conclusion

In summary, we have synergistically tailored the morphology and surface vacancies of the ECL emitter, and successfully synthesized 2D ultrathin Lu_2O_3–S nanosheets with abundant oxygen vacancies, which showed an intense and stable ECL intensity. Taking Lu_2O_3–S ultrathin nanosheets as novel ECL luminophores in cytosensing, further combining with DNA device cycle-amplification technology, an efficient, sensitive and specific method for CTCs counting method was established. With unique planar structure and large active sites, the Lu_2O_3–S ultrathin nanosheets has high carrier mobility and loading capacity, which also benefits the immobilization of biological recognition molecules and the construction of bioassay platform. The developed ECL cytosensing showed good sensitivity and selectivity, providing an alternative and considerable method for clinical tumor cells analysis. Compared with other ECL biosensors based on novel nanomaterials, the proposed ECL cytosensing platform exhibited better analytical performance, which can contribute to the promotion of electrochemiluminophores. The design thought of the newly prepared abundant oxygen vacancies contained 2D nanosheets emitter has a promising prospect in developing efficient electrochemiluminophores, and is beneficial for ECL-based clinical diagnosis.

Credit roles

Huan Gao: Conceptualization, Methodology, Formal analysis, Writing – original draft. Junfang Zhang: Data curation, Formal analysis. Xuan Wei: Visualization, Investigation., Qinshu Zhu: Supervision, Validation. Wei Tianxiang: Writing- Reviewing and Editing, Supervision, Funding acquisition.

Declaration of competing interest

The authors declare no competing financial interest.

Acknowledgements

This work was supported by the National Natural Science Foundation of China for the project (21705079, 21974070, and 22074064), the Natural Science Foundation of Jiangsu Province (BK20171033). We appreciate the financial support from the Priority Academic Program Development of Jiangsu Higher Education Institutions, the Program for Jiangsu Collaborative Innovation Center of Biomedical Functional Materials, and the Nanjing Science and Technology Innovation Project for Selected Overseas Chinese Scholar.

Appendix A. Supplementary data

Supplementary data to this article can be found online at https://doi.org/10.1016/j.talanta.2021.122230.

References

[1] Y. Wang, S. Sun, Z. Zhang, D. Shi, Nanomaterials for cancer precision medicine, Adv. Mater. 30 (17) (2018), e1705660, https://doi.org/10.1002/adma.201705660.
[2] F. Ye, Y. Zhao, R. El-Sayed, M. Muhammed, M. Hassan, Advances in nanotechnology for cancer biomarkers, Nano Today 18 (2018) 103–123, https://doi.org/10.1016/j.nantod.2017.12.008.
[3] V. Plaks, C.D. Koopman, Z. Werb, Circulating tumor cells, Science 341 (2013) 1186–1188, https://doi.org/10.1126/science.1235226.
[4] W. Li, H. Wang, Z. Zhao, H. Gao, C. Liu, L. Zhu, C. Wang, Y. Yang, Emerging nanotechnologies for liquid biopsy: the detection of circulating tumor cells and extracellular vesicles, Adv. Mater. 31 (45) (2019), e1805344, https://doi.org/10.1002/adma.201805344.
[5] Z. Shen, A. Wu, X. Chen, Current detection technologies for circulating tumor cells, Chem. Soc. Rev. 46 (2017) 2038–2056, https://doi.org/10.1039/c6cs00803h.
[6] V. Ortiz, M. Yu, Analyzing circulating tumor cells one at a time, Trends Cell Biol. 28 (2018) 764–775, https://doi.org/10.1016/j.tcb.2018.05.004.
[7] L. Xue, Z. Lyu, Y. Luan, X. Xiong, J. Pan, G. Chen, H. Chen, Efficient cancer cell capturing SiNWAs prepared via surface-initiated SET-LRP and click chemistry, Polym. Chem. 6 (2015) 3708–3715, https://doi.org/10.1039/c5py00247h.
[8] Z. Li, G. Wang, Y. Shen, N. Guo, N. Ma, DNA-templated magnetic nanoparticle-quantum dot polymers for ultrasensitive capture and detection of circulating tumor cells, Adv. Funct. Mater. 28 (2018) 1707152, https://doi.org/10.1002/adfm.201707152.
[9] M. Dervisevic, M. Senel, T. Sagir, S. Isik, Highly sensitive detection of cancer cells with an electrochemical cytosensor based on boronic acid functional polythiophene, Biosens. Bioelectron. 90 (2017) 6–12, https://doi.org/10.1016/j.bios.2016.10.100.
[10] J. Cao, X.P. Zhao, M.R. Younis, Z.Q. Li, X.H. Xia, C. Wang, Ultrasensitive capture, detection, and release of circulating tumor cells using a nanochannel-ion channel hybrid coupled with electrochemical detection technique, Anal. Chem. 89 (2017) 10957–10964, https://doi.org/10.1021/acs.analchem.7b02765.
[11] S. Xie, Y. Dong, Y. Yuan, Y. Chai, R. Yuan, Ultrasensitive lipopolysaccharides detection based on doxorubicin conjugated n-(aminobutyl)-n-(ethylisoluminol) as electrochemiluminescence indicator and self-assembled tetrahedron DNA dendrimers as nanocarriers, Anal. Chem. 88 (10) (2016) 5218–5224, https://doi.org/10.1021/acs.analchem.6b00276.
[12] M.M. Richer, Electrochemiluminescence (ECL) 104 (2004) 3003–3036, https://doi.org/10.1021/cr020373d.
[13] X. Wang, M. Zhang, X. Huo, W. Zhao, B. Kang, J.J. Xu, H. Chen, Modulating the electronic structure of a semiconductor to optimize its electrochemiluminescence performance, Nanoscale Adv 1 (2019) 1965–1969, https://doi.org/10.1039/c9na00011a.
[14] Y. Chen, S. Zhou, L. Li, J.J. Zhu, Nanomaterials-based sensitive electrochemiluminescence biosensing, Nano Today 12 (2017) 98–115, https://doi.org/10.1016/j.nantod.2016.12.013.
[15] F. Wang, J. Lin, T. Zhao, D. Hu, T. Wu, Y. Liu, Intrinsic "vacancy point defect" induced electrochemiluminescence from coreless supertetrahedral chalcogenide nanocluster, J. Am. Chem. Soc. 138 (2016) 7718–7724, https://doi.org/10.1021/jacs.6b03662.
[16] R. Wang, H. Wu, R. Chen, Y. Chi, Strong electrochemiluminescence emission from oxidized multiwalled carbon nanotubes, Small 15 (2019), e1901550, https://doi.org/10.1002/smll.201901550.
[17] H. Peng, Z. Huang, Y. Sheng, X. Zhang, H. Deng, W. Chen, J. Liu, Pre-oxidation of gold nanoclusters results in a 66% anodic electrochemiluminescence yield and drives mechanistic insights, Angew. Chem. 58 (2019) 11691–11694, https://doi.org/10.1002/anie.201905007.
[18] X. Long, F. Zhang, Y. He, S. Hou, B. Zhang, G. Zou, Promising anodic electrochemiluminescence of nontoxic core/shell $CuInS_2$/ZnS nanocrystals in aqueous medium and its biosensing potential, Anal. Chem. 90 (2018) 3563–3569, https://doi.org/10.1021/acs.analchem.8b00006.
[19] H. Li, Y. Li, A. Aljarb, Y. Shi, L.J. Li, Epitaxial growth of two-dimensional layered transition-metal dichalcogenides: growth mechanism, controllability, and scalability, Chem. Rev. 118 (2018) 6134–6150, https://doi.org/10.1021/acs.chemrev.7b00212.
[20] Y. Chen, C. Tan, H. Zhang, L. Wang, Two-dimensional graphene analogues for biomedical applications, Chem. Soc. Rev. 44 (2015) 2681–2701, https://doi.org/10.1039/c4cs00300d.
[21] X. Li, X. Sun, D. Fan, T. Yan, R. Feng, H. Wang, D. Wu, Q. Wei, A ternary quenching electrochemiluminescence insulin immunosensor based on Mn^{2+} released from MnO_2@Carbon core-shell nanospheres with ascorbic acid quenching AuPdPt-MoS_2@TiO_2 enhanced luminol, Biosens. Bioelectron. 142 (2019) 111551, https://doi.org/10.1016/j.bios.2019.111551.
[22] W. Gao, Z. Liu, L. Qi, J. Lai, S.A. Kitte, G. Xu, Ultrasensitive glutathione detection based on lucigenin cathodic electrochemiluminescence in the presence of MnO_2 nanosheets, Anal. Chem. 88 (2016) 7654–7659, https://doi.org/10.1021/acs.analchem.6b01491.
[23] J.C.G. Bünzli, Lanthanide luminescence for biomedical analyses and imaging, Chem. Rev. 110 (2010) 2729–2755, https://doi.org/10.1021/cr900362e.
[24] Y. Zhao, R. Wei, X. Feng, L. Sun, P. Liu, Y. Su, L. Shi, Dual-mode luminescent nanopaper based on ultrathin g-C_3N_4 nanosheets grafted with rare-earth upconversion nanoparticles, ACS Appl. Mater. Interfaces 8 (2016) 21555–21562, https://doi.org/10.1021/acsami.6b06254.
[25] C. Tian, L. Wang, F. Luan, X. Fu, X. Zhuang, L. Chen, A novel electrochemiluminescent emitter of europium hydroxide nanorods and its application in bioanalysis, Chem. Commun. 55 (2019) 12479–12482, https://doi.org/10.1039/c9cc07129f.
[26] H. Gao, S. Liu, Z. Wang, L. Si, Z. Dai, A novel electrochemiluminescence biosensor based on S-doped yttrium oxide ultrathin nanosheets for the detection of anti-dig antibodies, Analyst 143 (2018) 2997–3000, https://doi.org/10.1039/c8an00667a.
[27] M. Weidner, A. Fuchs, T.J.M. Bayer, K. Rachut, P. Schnell, G.K. Deyu, A. Klein, Defect modulation doping, Adv. Funct. Mater. 29 (2019) 1807906, https://doi.org/10.1002/adfm.201807906.
[28] J. Cai, Y. Zhu, D. Liu, M. Meng, Z. Hu, Z. Jiang, Synergistic effect of titanate-anatase heterostructure and hydrogenation-induced surface disorder on photocatalytic water splitting, ACS Catal. 5 (2015) 1708–1716, https://doi.org/10.1021/acscatal.5b00055.
[29] W. Lv, L. Li, M. Xu, J. Hong, X. Tang, L. Xu, Y. Wu, R. Zhu, R. Chen, W. Huang, Improving the stability of metal halide perovskite quantum dots by encapsulation, Adv. Mater. 31 (2019) 1900682, https://doi.org/10.1002/adma.201900682.
[30] S. Bertolazzi, M. Gobbi, Y. Zhao, C. Backes, P. Samorì, Molecular chemistry approaches for tuning the properties of two-dimensional transition metal dichalcogenides, Chem. Soc. Rev. 47 (2018) 6845–6888, https://doi.org/10.1039/c8cs00169c.
[31] J.X. Wang, Y. Zhuo, Y. Zhou, H.J. Wang, R. Yuan, Y.Q. Chai, Ceria doped zinc oxide nanoflowers enhanced luminol-based electrochemiluminescence immunosensor for amyloid-beta detection, ACS Appl. Mater. Interfaces 8 (2016) 12968–12975, https://doi.org/10.1021/acsami.6b00021.
[32] X. Du, D. Jiang, L. Dai, W. Zhu, X. Yang, N. Hao, K. Wang, Oxygen vacancy engineering in europia clusters/graphite-like carbon nitride nanostructures induced signal amplification for highly efficient electrochemiluminesce aptasensing, Anal. Chem. 90 (2018) 3615–3620, https://doi.org/10.1021/acs.analchem.8b00162.
[33] Y. Du, J. Xue, X. Sun, D. Wu, X. Liu, H. Ju, L. Yang, Q. Wei, Oxygen vacancy-enhanced electrochemiluminescence sensing strategy using luminol thermally encapsulated in apoferritin as a transducer for biomarker immunoassay, Anal. Chem. 92 (2020) 8472–8479, https://doi.org/10.1021/acs.analchem.0c01238.
[34] X. Pang, C. Cui, M. Su, Y. Wang, Q. Wei, W. Tan, Construction of self-powered cytosensing device based on ZnO nanodisks@g-C_3N_4 quantum dots and application in the detection of CCRF-CEM cells, Nano energy 46 (2018) 101–109, https://doi.org/10.1016/j.nanoen.2018.01.018.
[35] T. Zheng, T. Tan, Q. Zhang, J.J. Fu, J.J. Wu, K. Zhang, J.J. Zhu, H. Wang, Multiplex acute leukemia cytosensing using multifunctional hybrid electrochemical nanoprobes at a hierarchically nanoarchitectured electrode interface, Nanoscale 5 (2013) 10360–10368, https://doi.org/10.1039/c3nr02903d.
[36] D. Shangguan, Y. Li, Z. Tang, Z.C. Cao, H.W. Chen, P. Mallikaratchy, K. Sefah, C. J. Yang, W. Tan, Aptamers evolved from live cells as effective molecular probes for cancer study, P. Natl. Acad. Sci. USA 103 (2006) 11838–11843, https://doi.org/10.1073/pnas.0602615103.
[37] M.S. Wu, L.J. He, J.J. Xu, H.Y. Chen, RuSi@$Ru(bpy)_3^{2+}$/Au@Ag_2S nanoparticles electrochemiluminescence resonance energy transfer system for sensitive DNA detection, Anal. Chem. 86 (2014) 4559–4565, https://doi.org/10.1021/ac500591n.
[38] H. Zhou, Y.Y. Zhang, J. Liu, J.J. Xu, H.Y. Chen, Electrochemiluminescence resonance energy transfer between CdS:Eu nancrystals and Au nanorods for sensitive DNA detection, J. Phys. Chem. C 116 (2012) 17773–17780, https://doi.org/10.1021/jp305076g.
[39] M.R. Awual, A facile composite material for enhanced cadmium(II) ion capturing from wastewater, J. Environ. Chem. Eng. 7 (5) (2019) 103378, https://doi.org/10.1016/j.jece.2019.103378.
[40] M.R. Awual, A novel facial composite adsorbent for enhanced copper(II) detection and removal from wastewater, Chem. Eng. J. 266 (2015) 368–375, https://doi.org/10.1016/j.cej.2014.12.094.
[41] M.R. Awual, M.M. Hasan, A ligand based innovative composite material for selective lead(II) capturing from wastewater, J. Mol. Liq. 294 (2019) 111679, https://doi.org/10.1016/j.molliq.2019.111679.
[42] M.R. Awual, Mesoporous composite material for efficient lead(II) detection and removal from aqueous media, J. Environ. Chem. Eng. 7 (3) (2019) 103124, https://doi.org/10.1016/j.jece.2019.103124.

[43] M.R. Awual, M.M. Hasan, H. Znad, Organic–inorganic based nano-conjugate adsorbent for selective palladium(II) detection, separation and recovery, Chem. Eng. J. 259 (2015) 611–619, https://doi.org/10.1016/j.cej.2014.08.028.
[44] M.R. Awual, M.M. Hasan, A. Islam, A.M. Asiri, M.M. Rahman, Optimization of an innovative composited material for effective monitoring and removal of cobalt(II) from wastewater, J. Mol. Liq. 298 (2020) 112035, https://doi.org/10.1016/j.molliq.2019.112035.
[45] M.R. Awual, Novel ligand functionalized composite material for efficient copper(II) capturing from wastewater sample, Compos. B Eng. 172 (2019) 387–396, https://doi.org/10.1016/j.compositesb.2019.05.103.
[46] M.R. Awual, M.M. Hasan, Novel conjugate adsorbent for visual detection and removal of toxic lead(II) ions from water, Microporous Mesoporous Mater. 196 (2014) 261–269, https://doi.org/10.1016/j.micromeso.2014.05.021.
[47] R. Li, W. Tu, H. Wang, Z. Dai, Near-infrared light excited and localized surface plasmon resonance-enhanced photoelectrochemical biosensing platform for cell analysis, Anal. Chem. 90 (2018) 9403–9409, https://doi.org/10.1021/acs.analchem.8b02047.
[48] J. Wang, H.S. Zhou, Aptamer-based Au nanoparticles-enhanced surface plasmon resonance detection of small molecules, Anal. Chem. 80 (2008) 7174–7178, https://doi.org/10.1021/ac801281c.
[49] M.R. Awual, Innovative composite material for efficient and highly selective pb(II) ion capturing from wastewater, J. Mol. Liq. 284 (2019) 502–510, https://doi.org/10.1016/j.molliq.2019.03.157.
[50] M.R. Awual, Efficient phosphate removal from water for controlling eutrophication using novel composite adsorbent, J. Clean. Prod. 228 (2019) 1311–1319, https://doi.org/10.1016/j.jclepro.2019.04.325.
[51] B. Liu, C. Li, G. Zhang, X. Yao, S.S.C. Chuang, Z. Li, Oxygen vacancy promoting dimethyl carbonate synthesis from CO_2 and methanol over Zr-doped CeO_2 nanorods, ACS Catal. 8 (2018) 10446–10456, https://doi.org/10.1021/acscatal.8b00415.
[52] T. Yang, J. Wei, Y. Guo, Z. Lv, Z. Xu, Z. Cheng, Manipulation of oxygen vacancy for high photovoltaic output in bismuth ferrite films, ACS Appl. Mater. Interfaces 11 (2019) 23372–23381, https://doi.org/10.1021/acsami.9b06704.
[53] Y. Liu, C. Ma, Q. Zhang, W. Wang, P. Pan, L. Gu, D. Xu, J. Bao, Z. Dai, 2D electron gas and oxygen vacancy induced high oxygen evolution performances for advanced Co_3O_4/CeO_2 nanohybrids, Adv. Mater. 31 (2019), e1900062, https://doi.org/10.1002/adma.201900062.
[54] S. Zhao, M. Li, M. Han, D. Xu, J. Yang, Y. Lin, N.-E. Shi, Y. Lu, R. Yang, B. Liu, Z. Dai, J. Bao, Defect-rich Ni_3FeN nanocrystals anchored on N-doped graphene for enhanced electrocatalytic oxygen evolution, Adv. Funct. Mater. 28 (18) (2018) 1706018, https://doi.org/10.1002/adfm.201706018.
[55] K. Zhang, C.G. Ma, J.Y. Zhang, B.M. Liu, Y. Zhou, S.Q. Guo, J.Y. Xu, J.S. Hou, Y. Z. Fang, L.R. Zheng, H.T. Sun, Giant enhancement of luminescence from phosphors through oxygen-vacancy-mediated chemical pressure relaxation, Adv. Optical Mater. 5 (20) (2017) 1700448, https://doi.org/10.1002/adom.201700448.
[56] G. Ou, Y. Xu, B. Wen, R. Lin, B. Ge, Y. Tang, Y. Liang, C. Yang, K. Huang, D. Zu, R. Yu, W. Chen, J. Li, H. Wu, L.M. Liu, Y. Li, Tuning defects in oxides at room temperature by lithium reduction, Nat. Commun. 9 (2018) 1302, https://doi.org/10.1038/s41467-018-03765-0.
[57] Y.M. Lei, W.X. Huang, M. Zhao, Y.Q. Chai, R. Yuan, Y. Zhuo, Electrochemiluminescence resonance energy transfer system: mechanism and application in ratiometric aptasensor for lead ion, Anal. Chem. 87 (2015) 7787–7794, https://doi.org/10.1021/acs.analchem.5b01445.
[58] Y. Li, Z.W. Jiang, S.Y. Xiao, C.Z. Huang, Y.F. Li, Terbium(III) organic gels: novel antenna effect-induced enhanced electrochemiluminescence emitters, Anal. Chem. 90 (2018) 12191–12197, https://doi.org/10.1021/acs.analchem.8b03383.
[59] S. Liu, Q. Zhang, L. Zhang, L. Gu, G. Zou, J. Bao, Z. Dai, Electrochemiluminescence tuned by electron-hole recombination from symmetry-breaking in wurtzite ZnSe, J. Am. Chem. Soc. 138 (2016) 1154–1157, https://doi.org/10.1021/jacs.5b12727.
[60] M.R. Awual, Novel conjugated hybrid material for efficient lead(II) capturing from contaminated wastewater, Mater. Sci. Eng. C 101 (2019) 686–695, https://doi.org/10.1016/j.msec.2019.04.015.
[61] M.R. Awual, Investigation of potential conjugate adsorbent for efficient ultra-trace gold(III) detection and recovery, J. Ind. Eng. Chem. 20 (5) (2014) 3493–3501, https://doi.org/10.1016/j.jiec.2013.12.040.